High spatial resolution mapping of surface velocities and depths for shallow overland flow

Cédric Legout, Frédéric Darboux, Yves Nedelec, Alexandre Hauet, Michel Esteves, Bernard Renaux, Hervé Denis, Stéphane Cordier

To cite this version:

Cédric Legout, Frédéric Darboux, Yves Nedelec, Alexandre Hauet, Michel Esteves, et al.. High spatial resolution mapping of surface velocities and depths for shallow overland flow. Earth Surface Processes and Landforms, 2012, 37 (9), pp.984-993. 10.1002/esp.3220 . hal-02651894

HAL Id: hal-02651894
https://hal.inrae.fr/hal-02651894

Submitted on 29 May 2020

Earth Surface Processes and Landforms, 2012, http://dx.doi.org/10.1002/esp.3220

High spatial resolution mapping of surface velocities and depths for shallow overland flow

C. Legout[1*], F. Darboux[2], Y. Nédélec[3], A. Hauet[4], M. Esteves[5], B. Renaux[2], H. Denis[6] and S. Cordier[7]

[1] *UJF-Grenoble 1 /CNRS / G-INP / IRD, LTHE UMR 5564, Grenoble, F-38041, France.*

[2] *INRA, UR0272, UR Science du sol, Centre de recherche d'Orléans, CS 40001, F-45075 Orléans Cedex 2, France.*

[3] *CETE du Sud-Ouest / Département Laboratoire de Bordeaux / Groupe Géotechnique, Risques et Bâtiments, Bordeaux, France*

[4] *EDF-Centre Hydrométéorologique Pyrénées Massif Central, Toulouse, France.*

[5] *IRD / UJF-Grenoble 1 / CNRS / G-INP, LTHE UMR 5564, Grenoble, F-38041, France*

[6] *CNRS / UJF-Grenoble 1 / G-INP / IRD, LTHE UMR 5564, Grenoble, F-38041, France*

[7] *CNRS / U Orléans / MAPMO, Orléans, France*

*

Corresponding author:
LTHE (UMR 5564), BP 53, 38041 Grenoble Cedex 09, FRANCE
Tel: +33 4 76 63 56 63
Fax: +33 4 76 82 50 01
E-mail: Cedric.Legout@ujf-grenoble.fr

Earth Surface Processes and Landforms, 2012, http://dx.doi.org/10.1002/esp.3220

1 Abstract

Point measurements of flow rate, depth or velocity are not sufficient to validate overland flow models, particularly when the interaction of the water with the soil surface creates a complex flow geometry. In this study, we present the coupling of two techniques obtaining spatial data of flow depths and surface velocity measurements for water depths as low as a one millimetre. Overland flow experiments were performed in the laboratory at various flow rates and slopes on two surfaces. The first surface was 120 cm by 120 cm showing three undulations of sinusoidal shape with an amplitude of 1 cm and a wavelength of 20 cm, while the second was a 60 cm by 60 cm moulded reproduction of a seedbed with aggregates up to 2 cm in size. Large scale particle image velocimetry (LSPIV) was used for velocity measurements with a sub-centimetre spatial resolution. An instantaneous-profile laser scanner was used to map flow depths with a sub-millimetre spatial resolution. A sensitivity analysis of the image processing of the LSPIV showed a good robustness of the method. Comparison with measurements performed with hot film anemometer and salt velocity gauge showed that LSPIV surface velocities were representative of the flow. Water depths measured with the laser scanner were also in good agreement with single-point measurements performed with a dial indicator. Spatially-distributed flow rates could be computed by combining both presented techniques with a mean relative error less than 20%.

Keywords: free surface hydraulics, shallow flow, overland flow, flow velocity, flow depth, particle image velocimetry, laser scanner.

Earth Surface Processes and Landforms, 2012, http://dx.doi.org/10.1002/esp.3220

2 Introduction

Excessive runoff may show such undesirable effects as erosion, siltation, or suspended load, responsible for water quality degradation. Hydraulic and hydrologic tools are needed to help evaluate and mitigate such effects whenever it is possible. However, it is clear that, at present, our ability to model water and associated sediment discharge in small watersheds is largely inaccurate (Mitas and Mitasova, 1998; Nearing, 1998; Jetten et al., 1999; Jetten et al., 2003; Beven, 2006). This may be due in large part to the focus on what occurs at the catchment outlet (Jetten et al., 1999) and to the associated strong likelihood to predict the correct results for the wrong reasons (Favis-Mortlock et al., 1996, Jetten et al., 1996, Takken et al., 1999) which refers to the equifinality concept (Beven, 1989).

Within a watershed, the spatial and temporal distribution of overland flow is controlled by the interactions between objects of various spatial scales such as topography, ridge-and-furrow geometry created by agricultural work within the fields, random roughness generated by clods or aggregates, and ditches and the hydrographic network. While the flow pattern is clearly the result of the interaction between these objects, the way they interact remains mostly unspecified. Particularly, our knowledge of the interactions between topography and agricultural patterns is quite limited (Govers et al., 2000). Agricultural patterns, such as ridge-and-furrow geometry, create at the soil surface a particular shape that may act on overland flow as an obstacle as well as, oppositely, a straight channel. At low flux, the flow direction is controlled by the ridge-and-furrow direction only. For higher fluxes, when the water reaches the top of the ridges (height of approximately 1 to 10 cm), water flows in the direction of the topographic slope too. Up to now this dual behaviour is only addressed through empirical laws based on field observations. This lead to on/off predictions where the predicted flow direction is either the topographic slope direction or the ridge-and-furrow direction (Souchère et al., 1998; Takken et al., 2001). Once implemented in hydrologic models, these empirical laws improve the prediction of the spatial runoff pattern (Souchère et al., 1998; Cerdan et al., 2002; Takken et al., 2001). Nevertheless such laws are limited by the range of situations encompassed and their non-dynamic prediction. These issues can be addressed using physically-based numerical models. However, high resolution measurements of both flow velocity and flow depth are required to test and validate overland flow models for various combinations of flow rates, slope angles and ridge-and-furrow directions.

Many technologies have been used to measure velocities of overland flow such as hot film anemometry (Abrahams and Li, 1998), acoustic Doppler velocimetry (Gimenez et al., 2004),

Earth Surface Processes and Landforms, 2012, http://dx.doi.org/10.1002/esp.3220

dye tracing (Profitt et al., 1991; Beuselinck et al, 1999) and salt tracing. This last technology is the most common with various levels of complexity or interpretation of the conductivity signal measured downstream (Luk and Merz, 1992; Li and Abrahams, 1996; Li and Abrahams, 1997; Parsons et al., 1998; Lei et al., 2005; Planchon et al., 2005). Techniques based on image analysis such as particle image velocimetry (PIV) allow access to velocities with a much higher spatial resolution than salt measurements (Adrian, 1991). Large scale particle image velocimetry (LSPIV), which is an extension of the conventional PIV technique and does not require expensive illumination or imaging devices (Meselhe et al., 2004), has already proved its efficiency to estimate flow velocity in rivers (Hauet et al., 2008, Muste et al., 2008) or in laboratory flumes (Nord et al., 2010). However, few studies applied this technique to very shallow water flows. A similar technique (Particle Tracking Velocimetry) was recently used by Sidorchuk et al. (2008) to estimate trajectories and velocities of soil aggregates transported by overland flow. To date, only Meselhe et al. (2004) report the use of an image-based method to estimate flow velocity showing that LSPIV has potential for measuring low velocities for water depths close to one millimetre.

Water depths of overland flow have also been measured using various techniques. Among these the Vernier point gauge (Lawrence, 2000), the caliper (Ciampalini and Torri, 1998), the graduated scale (Profitt et al., 1991), the time domain reflectometry (Schack-Kirchner et al., 2005) and the pressure gauge (Kinnell, 1988) all correspond to single-point measurements. Only the recent works of Huang et al. (2010) and Tal and Paola (2010) present a two-dimensional domain measurement of water depths. Both used a depth-from-luminosity technique, based on the optical properties of water mixed with a fluorescent dye, to map flow depth ranging from 1 to 5 mm (Huang et al., 2010) or 5 to 80 mm (Tal and Paola, 2010).

To the best of our knowledge no study on overland flow reported high spatial resolution measurements efforts dedicated to both flow velocities and water depths. Yet they are crucial data because comparisons of different overland flow models to point data on a plot show that one variable – velocity or depth – can be simulated fairly well, but no model is able to represent properly the patterns of both variables simultaneously (Tatard et al., 2008).

This paper presents and assesses the capabilities of two techniques that were used to obtain high spatial resolution mapping of flow depth and velocity for various flow rates, slopes, and microtopographies. LSPIV was used to obtain velocity maps of flowing areas with random roughness and ridge-and-furrow geometry. An instantaneous-profile laser scanner was used to measure water depths for the same flows.

Earth Surface Processes and Landforms, 2012, http://dx.doi.org/10.1002/esp.3220

3 Materials and methods

3.1 Laboratory setup

Two laboratory experimental setups with distinct sample surfaces are described (Figure 1). The first one was a sandy surface with a sinusoidal shape representing a ridge-and-furrow pattern (Figure 1a). The second surface was a mould of an agricultural seedbed which was much rougher and closer to a natural soil surface (Figure 1b). Velocity mapping by particle image velocimetry was tested on both surfaces while depth mapping by laser scanner was only applied to the first surface.

The first surface was a square of 120 cm by 120 cm, showing three corrugations of sinusoidal shape with an amplitude of 1 cm and a wavelength of 20 cm. The material was expanded polystyrene covered by a fibreglass layer with epoxy resin. Sand grains sieved between 0.05 and 0.1 cm were glued by the epoxy resin. The sand conferred hydrophilic properties to the surface and created hydraulic roughness. The water supply was located on the upper part of the surface. The inlet was 10 cm-wide and was set perpendicular to the direction of the largest slope. Input flow rates ranged from 6.5 to 8.0 L min^{-1}. The water input rate was chosen according to the general slope and the furrow slopes in order to have water flowing in 3 or 6 furrows without overflowing the last furrow. Flow rates were measured at steady-state, separately at the outlet of each corrugation by automatic weighing for 20 seconds to 2 minutes depending on the flux. The general slopes in the Y-direction ranged from 18 to 20%, whereas the slope in the X-direction was null. As the orientation of the corrugations with the Y-direction varied from one experiment to another, the slopes of the corrugations ranged from 0 to 3% (Table 1).

The second surface was a square of 60 cm by 60 cm made of a mix of resin and plaster. It was the moulded reproduction of a seedbed with aggregates up to 2 cm in size. Having been moulded on an actual agricultural field, this surface also showed a ridge-and-furrow pattern, with two 60 cm-long and 10 cm-wide furrows parallel to the X-axis. Overland flow experiments were conducted on this surface with flow rates ranging from 5.2 L min^{-1} to 10.9 L min^{-1} and slopes from 4 to 12% (Table 1). The water was supplied on the whole width of the surface by the overflowing of an upstream reservoir. The flow rates were measured by manual sample collection at the outlet every two minutes.

3.2 Surface velocity measurements

3.2.1 Image acquisition and pre-processing

Images were acquired using a high-speed digital camera (AOS MOTIONeer) with a 18-55 mm lens (NIKON). For frequencies ranging from 62.5 to 500 frames per second, the image size was 1280×1024 pixels. With a camera located at less than two metres above the studied surface, the average surface resolution was 0.56 millimetre. The image acquisition was controlled by commercial software (AOS imaging).

In order to get enough luminosity and images with sufficient contrast, two 800 W - 48 kHz projectors located downslope illuminated the surface with an angle of 60°. A diffusing paper was placed in front of each projector to prevent undesirable reflection.

After a few tests, ground black pepper was selected as tracer to measure surface velocity by image processing. For the experiments carried out on the white moulded surface the contrast with the black pepper was very good. Conversely, experiments on the sinusoidal sandy surface required water coloration with white dye to achieve sufficient contrast between tracers and the surface. It was achieved with titanium oxide at concentration levels of 3 to 5 g L^{-1}. Both manual and automatic tracer feeding methods were used successfully to obtain a density close to ten particles per square centimetre.

Because of lens distortion and viewing angles different from a nadir view, the recorded images in jpeg format were corrected using a two-dimensional projective transformation (Bradley et al., 2002; Hauet et al., 2008). Locations of check points of known coordinates were determined on the images. The transformation parameters were estimated by the method of least squares using an average of 6 to 8 check points.

3.2.2 Surface velocity calculation

The image-based approach uses the well known and effective laboratory flow measurement technique known as LSPIV. This technique estimates the movement of tracer particles between image pairs using a cross correlation analysis. The image processing software is based on the algorithm developed by Fujita et al. (1998). The procedure is based on the grey scale intensity of a group of pixels in each image named the interrogation area (IA). By moving the centre of the IA in a defined search area (SA) in the second image, the algorithm calculates the correlation (r) between the IA centred on a point a_{ij} in the first image and the IA centred at point b_{ij} in the second image taken with a time interval (T) as follows:

$$r\left(a_{ij},b_{ij}\right)=\frac{\sum_{i=1}^{Si}\sum_{j=1}^{Sj}\left[\left(A_{ij}-\overline{A_{ij}}\right)\left(B_{ij}-\overline{B_{ij}}\right)\right]}{\sqrt{\sum_{i=1}^{Si}\sum_{j=1}^{Sj}\left(A_{ij}-\overline{A_{ij}}\right)^2}\sqrt{\sum_{i=1}^{Si}\sum_{j=1}^{Sj}\left(B_{ij}-\overline{B_{ij}}\right)^2}} \tag{1}$$

where S_i and S_j are the sizes (in pixels) of the interrogation areas, A_{ij} and B_{ij} are the distributions of grey-level intensities in the two interrogation areas, and $\overline{A_{ij}}$ and $\overline{B_{ij}}$ the corresponding mean values of grey-level intensities. Among the correlation coefficients calculated within each point of the search area, the maximum is assumed to be the most probable displacement of the fluid from point a_{ij} between both images. Knowing the time interval (T) between the two images, velocity vectors are derived from the displacement vectors for each pair of images. Filtering is then performed by applying a minimum correlation threshold, r_{min}, on the r values in order to keep only velocity vectors that are assumed to be correct. Finally, a mean velocity and the associated standard deviation are calculated for the set of processed images.

Earth Surface Processes and Landforms, 2012, http://dx.doi.org/10.1002/esp.3220

3.2.3 Sensitivity analysis of the image processing step

Since image processing requires a certain expertise to determined some parameters (IA, r_{min}, T, number of images)*, *we assessed the sensitivity of the* LSPIV *method to this parameterisation during experiment B on the moulded surface (Table 1). The sensitivity analysis consisted in changing a parameter value from the reference value one at a time. Based on the expert knowledge of the image processing step, a set of "ideal" parameters was defined as a reference: *IA* was fixed to 20 pixels, r_{min} to 0.7, *T* to 6 ms and the number of images to 40. The variation of each parameter value from this reference was expressed in percentage. The impact of these changes was assessed on two outputs. First, we defined three zones (2 cm × 2 cm) on the moulded surface. Since the image processing step calculated a velocity vector every 0.5 cm in the X- and Y-directions, the number of velocity vectors obtained on each zone was 25. The mean velocities calculated from the 25 velocity vectors on each of the three zones were 8.5, 15.5 and 23 cm s^{-1}. Mean velocities obtained on each zone after a parameter change were compared to those obtained with the reference parameters, the variations being expressed in percentage. Second, we completed this analysis on single-point velocity values by an analysis on all the velocity vectors calculated on the imaged surface (i.e. with wet and dry zones). This consisted of comparing the number of velocity vectors with values higher than 10 cm s^{-1} obtained for the reference parameters with those obtained after a parameter variation. This additional check is evidently not enough to completely describe changes in the velocity distribution but this is a useful complement to the comparisons of single-point velocities.

3.3 Depth measurement

Depth measurements were achieved using the instantaneous-profile laser scanner described in Darboux and Huang (2003). This instrument was initially designed to measure the micro-topography of soil surfaces both indoor and outdoor. It uses triangulation principle to measure locations in x, y and z. A laser line and a CCD-array camera are used together: Two laser diodes (3.6-mW each. Wavelength of 635 nm) illuminates a single narrow line on the surface. This line is set in the field of view of the CCD-array camera with an oblique angle. The laser line is identified automatically on the camera picture as a set of pixels with high intensity values. Based on a calibration table, picture coordinates (row and column) are converted to

Earth Surface Processes and Landforms, 2012, http://dx.doi.org/10.1002/esp.3220

spatial coordinates (x and z), giving instantaneously elevation variations along a profile (the laser line). A map of surface elevations is created by recording profiles at regularly spaced locations. In its standard configuration, the laser scanner allows for the mapping of a surface with a resolution of about 0.5 mm in all three directions on a regular grid of 0.5 mm spacing in x and y. Profiles can be acquired at a frequency of 5 Hz. The device has an accuracy of about 0.5 mm in all directions.

To measure water depths, the profile computation algorithm of Darboux and Huang (2003) had to be modified. In its original design, pixels were considered as belonging to the laser line when light intensity exceeded a pre-defined threshold. Preliminary trials showed that this method did not enable us to get accurate measurements of the heights of water surface. The algorithm was modified and pixels having the highest intensity in each column of the image were considered as belonging to the laser line. This modification produced more accurate elevation measurements; however, data acquisition was more sensitive to ambient light and required almost complete darkness.

To carry out depth measurements, two elevation maps were acquired successively. First, the dry surface was scanned. Then, water was added and another scan was acquired. To be able to measure the heights of water surface, titanium oxide at low concentration (as low as 1 g L^{-1}) was added to the water. The titanium oxide particles reflected the laser light, ensuring the strongest light intensity received by the camera came from the water surface and not from the bottom. Although the laser light intensity received by the camera was lower for the water surface than for the dry surface, the concentration of titanium oxide was large enough to ensure the identification of the laser line on the water surface. The water depth was computed by subtracting the two acquired elevation datasets (water surface measurement and dry surface measurement).

3.4 Benchmark using single-point measurements

3.4.1 Flow velocity

Two measurement devices were used to assess the performance of the LSPIV method. During experiment A (Table 1), velocity profiles were measured using a hot film anemometer. The DANTEC Mini CTA 54T30 anemometer was mounted on a quartz fibre sensor 70 µm in diameter and 3 mm in length, covered by a nickel thin film of approximately 0.1 µm thick allowing measuring velocities ranging from 0.01 to 10 m s^{-1}. 30 velocity measurements were obtained at several depths and locations in the two furrows parallel to the X-axis on the moulded surface.

An automated salt-tracing gauge developed by Planchon et al. (2005) was used during experiments D and E. It allowed measurements on a short control section (3 cm) with an accuracy of about 1.5 cm s^{-1}.

3.4.2 Flow depth

To assess their accuracies, water depths measured with the laser scanner were compared with water depths measured with a dial indicator. The resolution of the dial indicator was 10^{-5} m. For a defined location, the water depth was measured manually with the dial indicator by taking one reading at the water surface (Z_{water}) and one reading at the water bottom ($Z_{surface}$). The associated (x,y) coordinates were measured manually. 32 depth measurements were taken with the dial indicator during experiments B and C and 18 were taken during experiments D and E (Table 1) to compare with the laser-scanner measurements.

3.4.3 Concordance between methods

Passing and Bablok regression (PBR) was used to estimate the agreement or possible systematic bias between measurement methods. PBR is a robust, non-parametric and non sensitive method to distribution of errors and data outliers (Passing and Bablok, 1983). After testing a linear relationship between measurements performed with instruments X and Y confidence intervals (CI) of 95% are calculated for the slope β and the intercept α. Lower and upper CI are used to determine whether there is only a chance difference between β and l and between α and 0. Thus, if 95% CI for α includes 0 it can be concluded that there is no significant difference between obtained α value and 0 and there is no constant difference between two methods. Respectively, if 95% CI for β includes 1, it can be concluded that there is no significant difference between obtained β value and 1 and there is no proportional difference between two methods. In such case we can assume that there is no significant difference between methods.

3.5 Flow rate calculation

The calculated flow rates, *Qcalc* (m^3 s^{-1}) for various transects on both studied surfaces were obtained from the flux of surface velocities through the whole water column as follows:

$$Qcalc=\sum_{y=i}^{y=j} {}_{y}\left(Zwater_{y}-Zsurface_{y}\right) \tag{2}$$

with $VsurfPIV_y$ (m s^{-1}) the flow surface velocity measured by the LSPIV method at each y coordinate from i to j metre along a given X-coordinate transect, $Zsurface_y$ (m), the height of the surface measured every Δy (m) and $Zwater_y$ (m), the height of the water surface. Doing that, we assumed that *VsurfPIV* was representative of the mean velocity of the flow. Δy values were 0.005 m and 0.01 m on the moulded surface and sinusoidal surface, respectively. *Z* values were measured with either the dial indicator for the flow rate calculations on the moulded surface or the laser scanner for calculations on the sinusoidal surface.

4 Results and discussion

4.1 Flow velocities

4.1.1 Sensitivity of the image processing step

Data show a satisfying robustness of the LSPIV parameterisation since velocities had a quite low sensitivity (20%) to a variation range of +/- 50% for main LSPIV parameters (Figure 2). The velocities were quite insensitive to the number of images and the size of the *IA*. The *IA* size, which defines the spatial resolution of the measurement, was chosen small enough to preserve the largest range of observations in flow since any flow pattern smaller than *IA* size is lost by image processing. However, it had to be large enough to include recognizable tracer patterns inside it, i.e. to encompass one or more of the "typical patterns" used to trace free surface flow. The minimum correlation coefficient required, r_{min}, had also few effects on the final velocity values except when it became greater than 0.8. When the matching criterion was too demanding, either the velocities at specific locations (Figure 2a, b, c) or the velocity distribution on the whole surface (Figure 2d) were significantly modified. In the range of values tested for the time interval *T* between two images, the velocities were actually most affected when *T* was decreased, i.e. when the sampling frequency was increased. This was observed particularly for low velocities. A decrease of *T* directly affected the ability of the image processing to catch the very small displacements of tracer from one image to the next. Finally, five images were sufficient to obtain correct velocity vectors. With $T = 6$ ms, velocity measurements were averaged over 30 ms; an acceptable interval for transient flow experiments.

Earth Surface Processes and Landforms, 2012, http://dx.doi.org/10.1002/esp.3220

4.1.2 Performance assessment of the LSPIV

The performance of the LSPIV method was assessed in three different ways. First, surface velocities measured by the LSPIV method, *VsurfPIV*, were compared with velocities, *Vsalt*, measured by the salt velocity gauge on the sinusoidal surface (Figure 3). The PBR analysis showed that there was a proportional difference between both methods. Most surface velocities measured by the LSPIV method were higher than those measured by the salt velocity gauge with a mean ratio *Vsalt/VsurfPIV* of 0.81 (Table 2). Second, surface velocity measurements were validated by comparing overall flow rates (*Qmeas*) measured manually during 30 s at the single outlet of the moulded surface (experiments B and C in Table 1) to flow rates (*Qcalc*) evaluated with equation 2. The calculated flow rates were close to those measured manually but systematically higher, with *Qcalc* values of 6.3, 11.3 and 12.4 L min^{-1}, respectively for Figure 4a, 4b and 4c, which was also in good agreement with the previous comparison of the velocities. Finally, we assessed the ability of surface velocity measurements to represent the velocities within the water column (Figure 5). The subvertical uniform velocity profiles obtained with the hot film anemometer agreed with results from previous studies with a similar technique (e.g. Abrahams and Li, 1998) and also with the results of both previous comparisons. Indeed, from Figure 5 we calculated ratios between weighted mean velocities on the whole profile ($Vanem_{MW}$) and velocities close to the water surface ($Vanem_{surf}$), leading to a mean value of 0.83.

The mean ratios derived from Figures 3, 4 and 5 and summarised in Table 2 were all comprised between 0.8 and 0.9 and could not be considered as significantly different according to the standard errors. Surface velocities were therefore considered as good indicators of the mean flow velocity, even if in some cases, the velocities may decrease close to the bed (Figure 5).

4.1.3 Limits

The limitations associated to the LSPIV technique were related to the tracer behaviour and the image acquisition. Concerning the tracers, the ratio of the tracer size and flow depth could be limiting particularly for zones with a very thin water film. However, because of its organic composition (i.e. low density of 0.55 g cm^{-3} and hydrophobicity), and a median grain size of 1 mm, ground black pepper remained on the flow surface without clustering and did not get snagged when water depths were higher than 0.5 mm. Once the tracer was chosen, the feeding step was also crucial since the area of interest had to be correctly covered by the tracer. As suggested by Mesehle et al. (2004), images selected for the LSPIV post processing

Earth Surface Processes and Landforms, 2012, http://dx.doi.org/10.1002/esp.3220

showed tracer density between 10 and 30% of the wetted surface and spread over the entire wetted surface.

The resolution of the camera was also a limit during the image acquisition step. Under our experimental conditions the imaged surface could not be larger than 0.5×0.7 m². Thus the plot was divided in three zones that were imaged and treated separately. Even if the acquisition step was relatively fast, this could have been a limitation to obtain data with a single camera on wide areas during transient flow conditions. This could be alleviated by using multiple cameras. Another limitation was the range of velocity that could have been measured. For our experimental conditions, characterised by highly nonuniform flows, the highest velocities dictated the appropriate sampling frequency (125 frames per second). To assess the lowest velocity that can be measured with this frequency, we used data from a flow experiment on the sinusoidal surface. During this experiment the flow was localised in the corrugations and thus no movement took place on the rest of the image, i.e. dry areas. However the velocities obtained with the LSPIV procedure on those dry areas were different from 0 (Figure 6). This allowed us to estimate a lower limit around 0.4 cm s^{-1} for U and V components for a time T of 8 ms between two images. This limit corresponded to the maximum values calculated on the immobile zones. It could be decreased reasonably since the 95% percentile is 0.13 cm s^{-1} for both U and V components. It could also be reduced by increasing the time between two images (Mesehle et al., 2004). Indeed the 95% percentile decreased to 0.06 cm s^{-1} for both U and V components when considering a 16 ms time period between two images (Figure 6) without modifying significantly the velocity vectors in the mobile zones. This means that a frequency sampling of 62.5 frames per second was sufficient for that flowing experiment. Thus it shows that the LSPIV procedure made it possible to optimise *a posteriori* the measurement accuracy.

4.2 Flow depths

Earth Surface Processes and Landforms, 2012, http://dx.doi.org/10.1002/esp.3220

4.2.1 Performance assessment

The PBR analysis revealed no significant difference between the measurements performed with the dial indicator and the laser scanner; yet Figure 7 shows that the laser scanner underestimated flow depth by roughly 0.5 mm. The regression line is almost parallel to the 1:1 line, thus the bias did not depend much of the water depth. This bias should be considered small since the accuracy of the laser scanner setup is 0.5 mm. The origin of this bias probably lied in the reflection of laser light by titanium oxide particles: because of the low particle concentration, the laser light could travel some distance inside the water layer before being reflected by a particle. Hence, the zone of most intense reflection was not exactly at the water surface but slightly below. Using a higher particle concentration could alleviate this problem, but it may also have affected the flow characteristics.

4.2.2 Capabilities and limits

From a practical point of view, the bias in the depth measurement means that depth measurements should be corrected by about 0.5 mm and that areas with water depth lower than 0.5 mm could not be differentiated from dry areas. The bias should be evaluated for each experimental setup since it will depend on the concentration of titanium oxide.

The method required the surface to create a diffuse reflection. If the surface was transparent, the camera could not locate the laser line. If the surface created a specular reflection (like a metallic surface), laser light could undergo multiple reflection before reaching the camera, leading to misidentifications in the location of the actual laser line. These limitations were not specific to the depth measurement procedure but to the original design of the instantaneous-profile laser scanner (Darboux and Huang, 2003).

Since the time needed to scan an area of 1 square metre was about 10 min., this technique could not be used to obtain time-dependent maps of flow depths varying under transient conditions. However, for experiments in which flow depth measurements along a single profile are relevant, it could be possible to acquire successive profiles at the same location with a rate of 5 Hz. It will simply require keeping the laser line from moving and enables to characterise transient flows. Since only single-point measurements are used in most published studies, using the laser-scanner technique with this setup may be a significant improvement in the understanding of transient flow properties and in the validation of numerical overland flow models.

Earth Surface Processes and Landforms, 2012, http://dx.doi.org/10.1002/esp.3220

4.3 Combining both methods

Both techniques were finally validated by comparing flow rates measured by automatic weighing to those obtained from the combination of laser scanner and LSPIV measurements. This comparison was performed for two experiments on the sinusoidal surface with distinct inflow rates, azimuths and slope angles, leading to water flowing on half of the corrugation outlets or on all the corrugation outlets. An example of raw measurements of velocities (obtained with LSPIV) and water depths (obtained with laser-scanner) is shown in Figure 8 for the experiment with three corrugations flowing. These raw data were used to calculate flow rates in each corrugation using equation 2 with a Δy value of 1 cm. For each corrugation, three transects were selected upstream from the corrugation outlet.

Figure 9 shows various water depth / surface velocity relationships in each corrugation. These relationships were substantially different from one experiment to another and also among the corrugations of a given experiment. We should stress that the velocity-depth relationships depended on the filling of the corrugation and its relative position from the water supply, showing the need to measure both depth and velocity with a high spatial resolution. As shown in Figure 10, the combination of both methods allowed us to obtain, under our experimental conditions, a mean relative error of 19% (St.Dev. = 10%) on the flux between reference and calculated values. The PBR analysis showed that there was no significant difference between the weighing method and the original method combining LSPIV and laser scanner.

Conclusion

In this study, we presented the coupling of two techniques allowing us to obtain spatial data of flow depth and surface velocity measurements for water depths ranging from a few millimetres to a few centimetres. The LSPIV procedure was a robust method to obtain surface velocity measurements with a relatively low sensitivity to parameter changes in a range of +/- 50% around "ideal" values based on the expert knowledge about the image processing step. The ratios between reference velocity values and LSPIV velocities were around 0.8-0.9 showing that the LSPIV slightly over-predicted the mean flow velocities but were representative of the flow. The minimum velocity value we could correctly measure under our experimental conditions was around 0.1 cm s^{-1}. The water depths measured by the laser-scanner were very well correlated to the reference values obtained with a dial indicator.

Earth Surface Processes and Landforms, 2012, http://dx.doi.org/10.1002/esp.3220

It should be noted that depth values were corrected since a 0.5 mm bias was observed. Finally the combination of both methods to obtain flow rates led to satisfactory results with a mean relative error less than 20%. Both techniques presented in this study are capable of producing data sets that are crucial to validate the hydrodynamics of plot scale overland-flow models and so to help in understanding the dynamics of soil erosion. Particularly it should allow for the parametrisation of Manning, Darcy-Weisbach or Chezy flow-resistance equations used in overland-flow and erosion models since hydrographs alone are insufficient sources of information.

Earth Surface Processes and Landforms, 2012, http://dx.doi.org/10.1002/esp.3220

References

Abrahams AD, Li G. 1998. Effect of saltating sediment on flow resistance and bed roughness in overland flow. *Earth Surface Processes and Landforms* **23**, 953-960.

Adrian RJ. 1991. Particle imaging techniques for experimental fluid mechanics. *Annual Reviews of Fluid Mechanics* **23**: 261-304.

Beuselinck L, Govers G, Steegen A, Hairsine PB, Poesen J. 1999. Evaluation of the simple settling theory for predicting sediment deposition by overland flow. *Earth Surface Processes and Landforms* **24**: 993-1007.

Beven K. 1989. Changing ideas in hydrology. The case of physically based models. *Journal of Hydrology* **105** (1-2): 157-172.

Beven K. 2006. On undermining the science? Hydrological Processes **20**: 2050-2065.

Bradley AA, Kruger A, Meselhe EA, Muste MVI. 2002. Flow measurement in streams using video imagery. *Water Resources Research* **8**(12): 1315.

Cerdan O, Souchère V, Lecomte V, Couturier A, Le Bissonnais Y. 2002. Incorporating soil surface crusting processes in an expert-based runoff model: STREAM (Sealing and Transfer by Runoff and Erosion related to Agricultural Management). *Catena* **46**: 189-205.

Ciampalini R, Torri D. 1998. Detachment of soil particles by shallow flow: sampling methodology and observations. *Catena* **32**: 37-53.

Darboux F, Huang C. 2003. An instantaneous-profile laser scanner to measure soil surface microtopography. *Soil Science Society of America Journal* **67**: 92-99.

Favis-Mortlock DT, Quinton JN, Dickinson WT. 1996. The GCTE validation of soil erosion models for global change studies. *Journal of Soil and Water Conservation* **51**(5): 397-403.

Fujita I, Muste M, Kruger A. 1998. Large-scale particle image velocimetry flow analysis in hydraulic engineering applications. *Journal of Hydraulic Research* **36**(3): 397-414.

Gimenez R, Planchon O, Silvera N, Govers G. 2004. Longitudinal velocity patterns and bed morphology interaction in a rill. *Earth Surface Processes and Landforms* **29**: 105-114.

Govers G, Takken I, Helming K. 2000. Soil roughness and overland flow. *Agronomie* **20**:131-146.

Hauet A, Kruger A, Krajewski WF, Bradley A, Muste M, Creutin JD, Wilson M. 2008. Experimental system for real-time discharge estimation using an image-based method. *Journal of Hydrologic Engineering* **13**(2): 105-110.

Huang MYF, Huang AYL, Capart H. 2010. Joint mapping of bed elevation and flow depth in microscale morphodynamics experiments. *Experiments in Fluids* **49**: 1121-1134.

Earth Surface Processes and Landforms, 2012, http://dx.doi.org/10.1002/esp.3220

Jetten V, Boiffin J, De Roo APJ. 1996. Defining monitoring strategies for runoff and erosion studies in agricultural catchments: a simulation approach. *European Journal of Soil Science* **47**: 579-592.

Jetten V, De Roo APJ, Favis-Mortlock D. 1999. Evaluation of field-scale and catchment-scale soil erosion models. *Catena* **37**: 521-541.

Jetten V, Govers G, Hessel R. 2003. Erosion models: quality of spatial predictions. *Hydrological Processes* **17**: 887-900.

Kinnell PIA. 1988. The influence of flow discharge on sediment concentrations in raindrop induced flow transport. *Australian Journal of Soil Research* **26**: 575-582.

Lawrence DSL. 2000. Hydraulic resistance in overland flow during partial and marginal surface inundation: Experimental observations and modeling. *Water Resources Research* **36**: 2381-2393.

Lei T, Xia W, Zhao J, Liu Z, Zhang Q. 2005. Method for measuring velocity of shallow water flow for soil erosion with an electrolyte tracer. *Journal of Hydrology* **301**: 139-145.

Li G, Abrahams AD. 1996. Correction factors in the determination of mean velocity of overland flow. *Earth Surface Processes and Landforms* **21**: 509-515.

Li G, Abrahams AD. 1997. Effect of saltating sediment load on the determination of the mean velocity of overland flow. *Water Resources Research* **33**(2): 341-347.

Luk SH, Merz W. 1992. Use of the salt tracing technique to determine the velocity of overland flow. *Soil Technology* **5**: 289-301.

Meselhe EA, Peeva T, Muste M. 2004. Large scale particle image velocimetry for low velocity and shallow water flows. *Journal of Hydraulic Engineering* **130**(9): 937-940.

Mitas L, Mitasova H. 1998. Distributed soil erosion simulation for effective erosion prevention. *Water Resources Research* **34**(3): 505-516.

Muste M, Fujita I, Hauet A. 2008. Large-scale particle image velocimetry for measurements in riverine environments. *Water Resources Research* **44**: W00D19 10.1029/2008WR006950.

Nearing MA. 1998. Why soil erosion models over-predict small soil losses and under-predict large soil losses. *Catena* **32**: 15-22.

Nord G, Esteves M, Lapetite JM, Hauet A. 2009. Effect of particle density and inflow concentration of suspended sediment on bedload transport in rill flow. *Earth Surface Processes and Landforms* **34**(2): 253-263.

Parsons AJ, Stromberg SGL, Greener M. 1998. Sediment-transport competence of rain-impacted interrill overland flow. *Earth Surface Processes and Landforms* **23**: 365-375.

Passing H, Bablok W. 1983. A new biometrical procedure for testing the equality of measurements from two different analytical methods. Application of linear regression procedures for method comparison studies in clinical chemistry, Part I. *Journal of Clinical Chemistry and Clinical Biochemistry* **21:** 709-720.

Planchon O, Silvera N, Gimenez R, Favis-Mortlock D, Wainwright J, Le Bissonnais Y, Govers G. 2005. An automated salt-tracing gauge for flow-velocity measurement. *Earth Surface Processes and Landforms* **30**: 833-844.

Proffitt APB, Rose CW, Hairsine PB. 1991. Rainfall detachment and deposition: experiments with low slopes and significant water depths *Soil Science Society of America Journal* **55**: 325-332.

Schack-Kirchner H, Schmid T, Hildebrand E. 2005. High-resolution monitoring of surface-flow depth with frequency-domain probes. *Soil Science Society of America Journal* **69**: 343-346.

Sidorchuk A, Schmidt J, Cooper G. 2008. Variability of shallow flow velocity and soil aggregate transport observed with digital videography. *Hydrological Processes* **22**: 4035-4048.

Souchère V, King D, Daroussin J, Papy F, Capillon A. 1998. Effects of tillage on runoff directions: consequences on runoff contributing area within agricultural catchments. *Journal of Hydrology* **206**: 256-267.

Takken I, Beuselinck L, Nachtergaele J, Govers G, Poesen J, Degraer G. 1999. Spatial evaluation of a physically based distributed erosion model (LISEM). *Catena* **37**: 431-447.

Takken I, Govers G, Jetten V, Nachtergaele J, Steegen A, Poesen J. 2001. The effect of tillage on runoff and erosion patterns. *Soil and Tillage Research* **61**: 55-60.

Tal M, Paola C. 2010. Effects of vegetation on channel morphodynamics: results and insights from laboratory experiments. *Earth Surface Processes and Landforms* **35**: 1014-1028

Tatard L, Planchon O, Wainwright J, Nord G, Favis-Mortlock D, Silvera N, Ribolzi O, Esteves M, Huang C. 2008. Measurement and modelling of high-resolution flow-velocity data under simulated rainfall on a low-slope sandy soil. *Journal of Hydrology* **348**: 1-12.

5 Acknowledgements

Earth Surface Processes and Landforms, 2012, http://dx.doi.org/10.1002/esp.3220

This work was supported by the ANR project METHODE #ANR-07-BLAN-0232 (http://www.univ-orleans.fr/mapmo/methode/). The authors wish to thank all the members of the project for fruitful discussions and for many helpful comments. They also thank Olivier Planchon (LISAH, IRD) for lending his salt velocity gauge. The authors are grateful to the two anonymous reviewers for their constructive comments that helped improving the manuscript.

Earth Surface Processes and Landforms, 2012, http://dx.doi.org/10.1002/esp.3220

6 List of figures

Figure 1: Laboratory devices: (a) 120 cm × 120 cm surface with a sinusoidal shape and (b) 130 cm-long and 60 cm-wide flume including a 60 cm × 60 cm mould of an agricultural soil surface.

The origins and directions of X and Y axes are indicated by black arrows for both studied surfaces.

Figure 2: Sensitivity of main LSPIV parameters assessed for a zone with (a) high velocity values, (b) medium velocity values, (c) low velocity values and also (d) on the basis of the number of vectors with values higher than 10 cm s^{-1}. Symbols are associated to the four LSPIV parameters tested. *Xref.* and *Yref.* are the reference values for the percentage of variation calculated respectively on both axes. Note that y-axis scale is different on each sub-figure.

Figure 3: Comparison of velocity values obtained with salt velocity gauge and LSPIV on the sinusoidal surface. Error bars are standard deviations. Equations in parentheses correspond to the Passing Bablok regression (PBR) line and the associated confidence intervals (CI).

Figure 4: Surface velocities and wetted section measured at an X-coordinate of 46.5 cm on the moulded surface for flow rates and slopes of respectively (a) 5.2 L min^{-1} and 7.3°, (b) 10.6 L min^{-1} and 4.4°, (c) 10.9 L min^{-1} and 2.3°. Surface velocities were measured with the LSPIV technique. Depths were measured with a dial indicator.

Figure 5: Velocity profiles and water depths measured by a hot film anemometer on several places of the moulded surface for various slopes (S) and flow rate (Q). Z corresponds to the measurement height while $Zwater$ corresponds to the height of the water surface. $Vanem$ corresponds to the velocity measured with hot film anemometer while $Vanem_{MW}$ corresponds to the weighted mean velocities on the whole profile. Error bars are standard deviations.

Figure 6: Values of velocity components U and V, along X- and Y-axes respectively, obtained with the LSPIV procedure on dry zones during flowing experiments on the

Earth Surface Processes and Landforms, 2012, http://dx.doi.org/10.1002/esp.3220

sinusoidal surface. The image processing was performed with a time interval between two images (*T*) of 0.008 or 0.016 s.

Figure 7: Comparison of water depth measurements with dial indicator and with laser scanner on the sinusoidal surface. Error bars are standard deviations. Equations in parentheses correspond to the Passing Bablok regression (PBR) line and the associated confidence intervals (CI).

Figure 8: Measurements of (a) flow velocity and (b) water depth for experiment D with three corrugations outflowing from the sinusoidal surface.

Figure 9: Velocity (LSPIV) and water depths (laser scanner) measured on various transects of each corrugation of the sinusoidal surface for two experiments. (a) Three outlets were active only on one side of the surface (Up, Central and Down). (b) All six outlets were flowing (i.e. both ends of each corrugation).

Figure 10: Comparison of flow rates obtained from automatic weighing and from the combination of laser scanner and LSPIV measurements for each corrugation on the sinusoidal surface. Error bars are standard deviations. Equations in parentheses correspond to the Passing Bablok regression (PBR) line and the associated confidence intervals (CI).

Version définitive du manuscrit publié dans / Final version of the manuscript published in :
Earth Surface Processes and Landforms, 2012, http://dx.doi.org/10.1002/esp.3220

7 List of tables

Table 1: Description of the various laboratory experiments.

Table 2: Comparison of velocity and flow rates ratios deduced from figures 3, 4 and 5.

Earth Surface Processes and Landforms, 2012, http://dx.doi.org/10.1002/esp.3220

Experiment	*Figure*	*Surface*	*Flow rate (L min^{-1})*	*Slope in the Y-direction (°)*	*Slope in the X-direction (°)*	*Measurements*
A	5	moulded	5 to 10	0.3 to 3	0.3 to 3	Velocity profiles: Hot film anemometer
B	2, 4c	moulded	10.9	2.3	2.3	Surface velocities: LSPIV Single-point water depth: dial indicator
C	4a, 4b	moulded	5.2 and 10.6	7.3 and 4.4	7.3 and 4.4	Surface velocities: LSPIV Single-point water depth: dial indicator
D	3, 6, 7, 9, 10a, 11	sinusoidal	6.5	11.3	3.2	Single-point velocity: salt gauge Surface velocities: LSPIV Water depths: laser scanner Single-point water depth: dial indicator
E	3, 7, 10b, 11	sinusoidal	8	10.2	0	Single-point velocity: salt gauge Surface velocities: LSPIV Water depths: laser scanner Single-point water depth : dial indicator

Table 1: Description of the various laboratory experiments.

Earth Surface Processes and Landforms, 2012, http://dx.doi.org/10.1002/esp.3220

Ratio	*Vsalt / VsurfPIV*			*Qcalc / Qmeas*			$Vanem_{MW} / Vanem_{surf}$		
Figure	*3*			*4*			*5*		
Statistics	*Mean*	*SE*	*n*	*Mean*	*SE*	*n*	*Mean*	*SE*	*n*
Value [-]	0.81	0.14	23	0.88	0.05	3	0.83	0.17	13

Table 2: Comparison of velocity and flow rates ratios deduced from figures 3, 4 and 5.

Earth Surface Processes and Landforms, 2012, http://dx.doi.org/10.1002/esp.3220

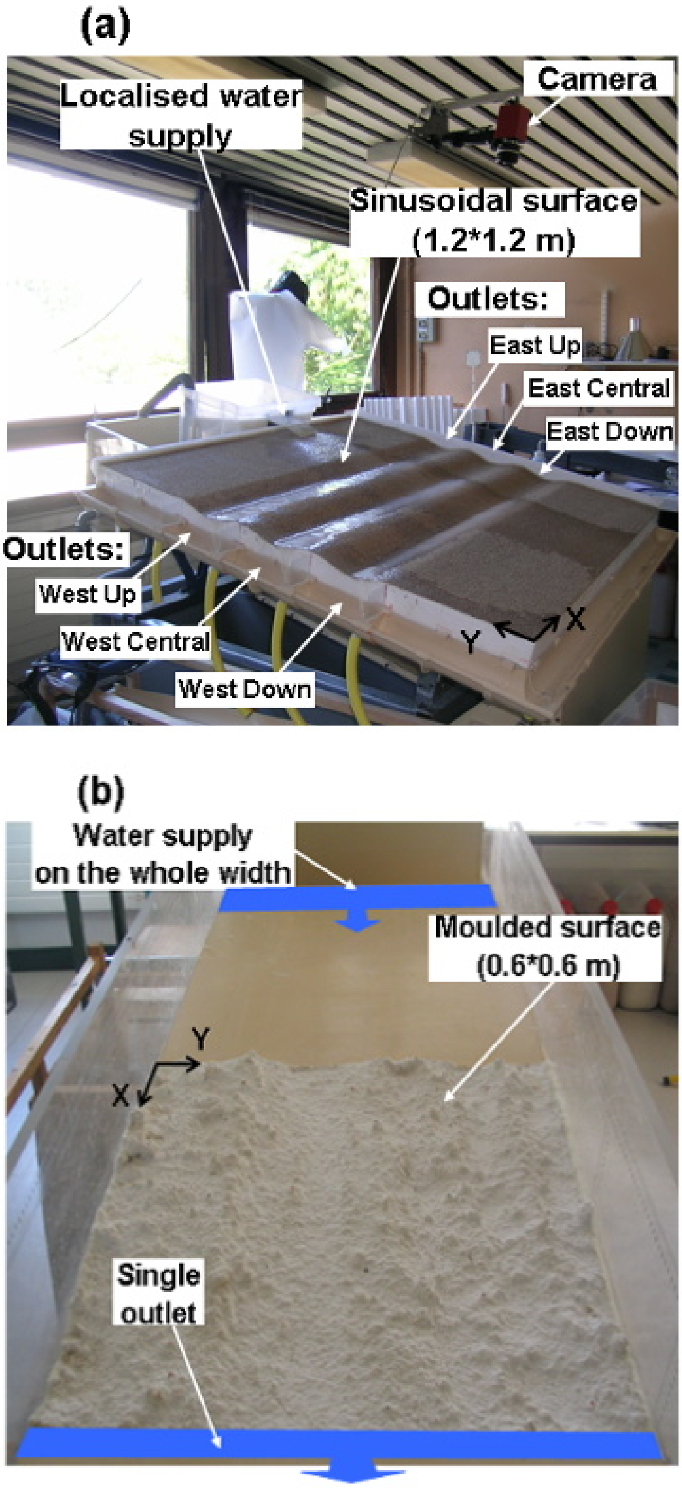

Figure 1: Laboratory devices: (a) 120 cm × 120 cm surface with a sinusoidal shape and (b) 130 cm-long and 60 cm-wide flume including a 60 cm × 60 cm mould of an agricultural soil surface.

The origins and directions of X and Y axes are indicated by black arrows for both studied surfaces.

Earth Surface Processes and Landforms, 2012, http://dx.doi.org/10.1002/esp.3220

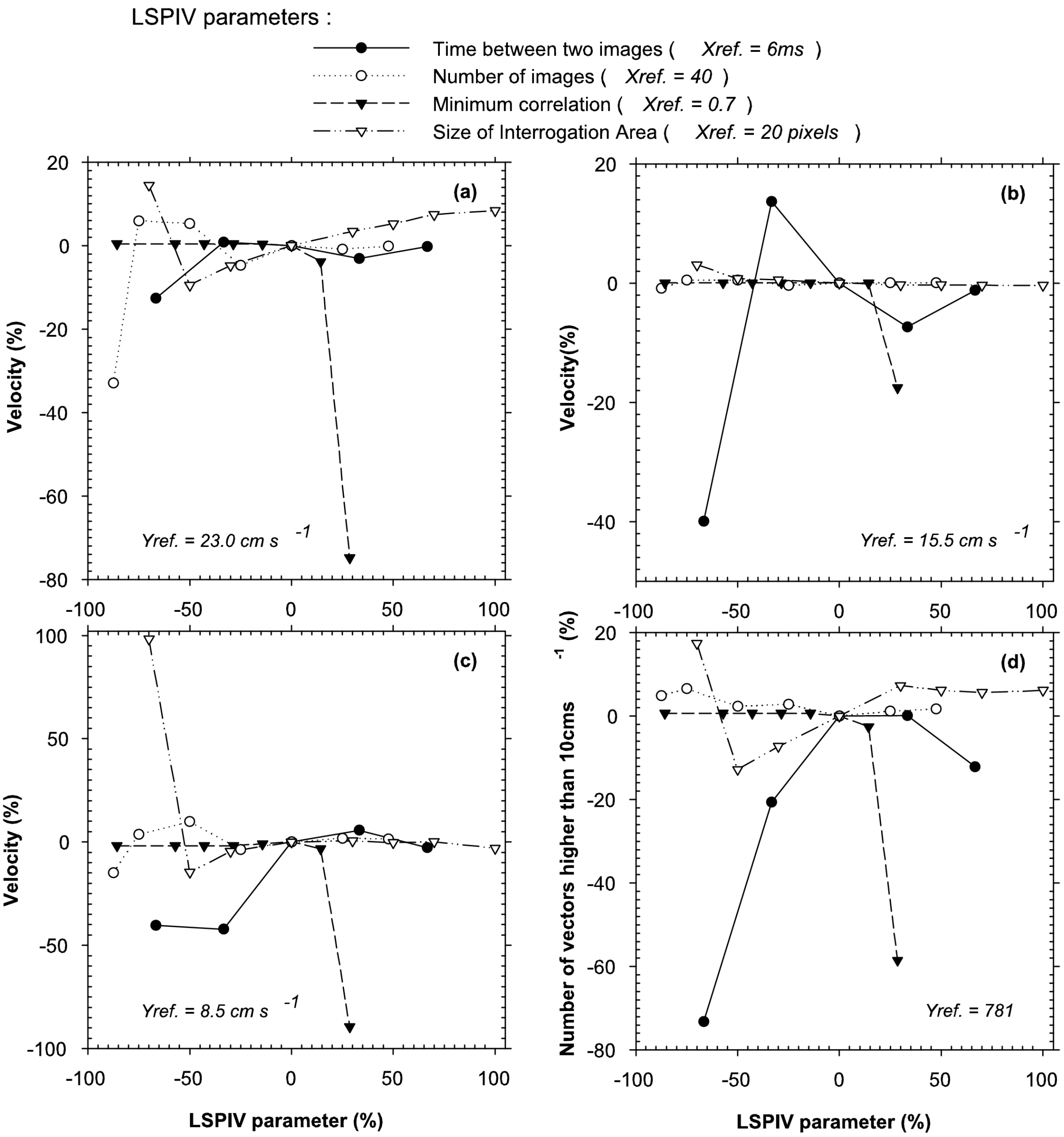

Figure 2: Sensitivity of main LSPIV parameters assessed for a zone with (a) high velocity values, (b) medium velocity values, (c) low velocity values and also (d) on the basis of the number of vectors with values higher than 10 cm s^{-1}. Symbols are associated to the four LSPIV parameters tested. *Xref.* and *Yref.* are the reference values for the percentage of variation calculated respectively on both axes. Note that y-axis scale is different on each sub-figure.

Earth Surface Processes and Landforms, 2012, http://dx.doi.org/10.1002/esp.3220

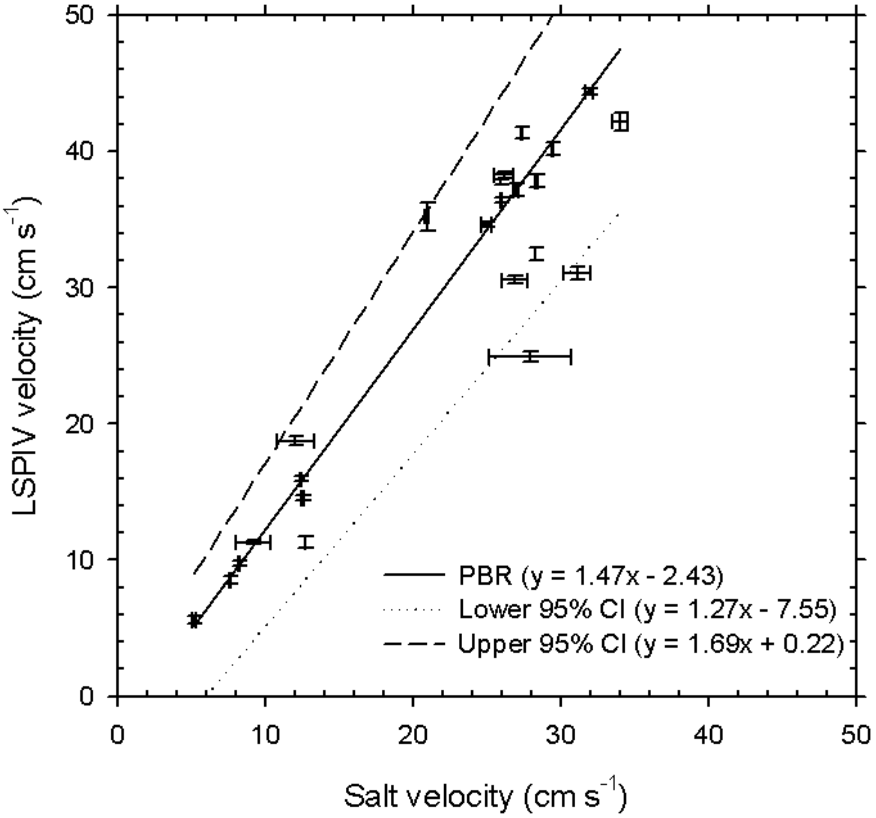

Figure 3: Comparison of velocity values obtained with salt velocity gauge and LSPIV on the sinusoidal surface. Error bars are standard deviations. Equations in parentheses correspond to the Passing Bablok regression (PBR) line and the associated confidence intervals (CI).

Earth Surface Processes and Landforms, 2012, http://dx.doi.org/10.1002/esp.3220

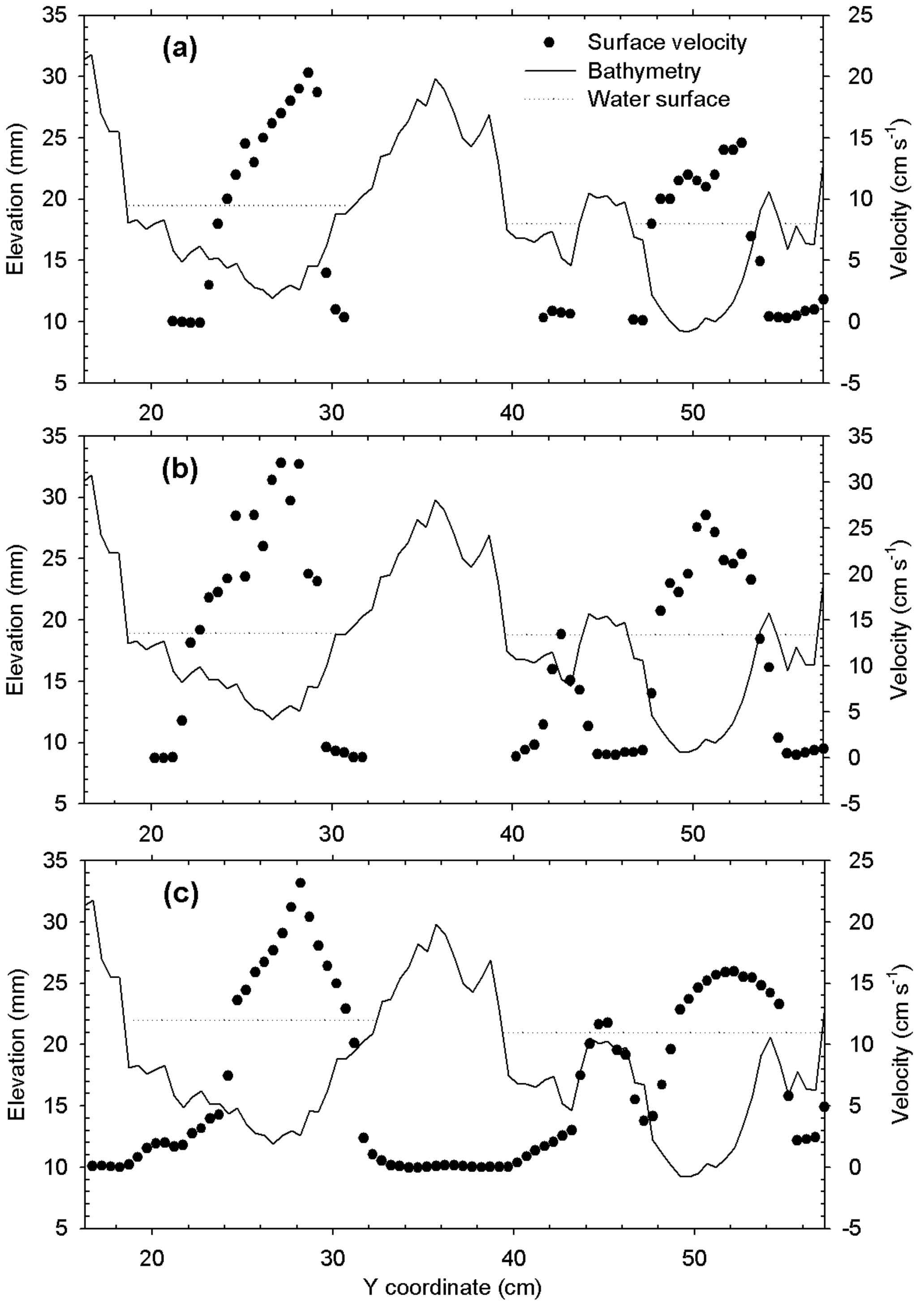

Figure 4: Surface velocities and wetted section measured at an X-coordinate of 46.5 cm on the moulded surface for flow rates and slopes of respectively (a) 5.2 L min^{-1} and 7.3°, (b) 10.6 L min^{-1} and 4.4°, (c) 10.9 L min^{-1} and 2.3°. Surface velocities were measured with the LSPIV technique. Depths were measured with a dial indicator.

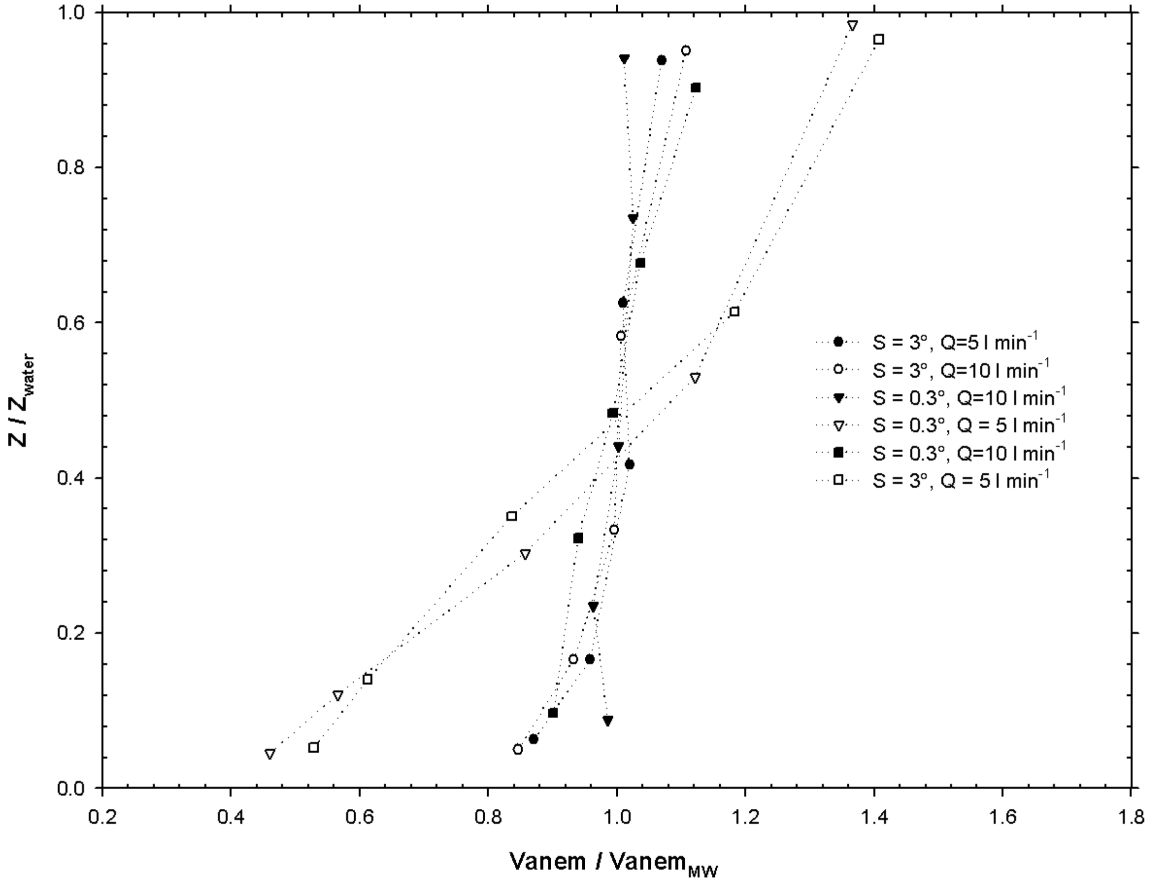

Figure 5: Velocity profiles and water depths measured by a hot film anemometer on several places of the moulded surface for various slopes (*S*) and flow rate (*Q*). *Z* corresponds to the measurement height while *Zwater* corresponds to the height of the water surface. *Vanem* corresponds to the velocity measured with hot film anemometer while $Vanem_{MW}$ corresponds to the weighted mean velocities on the whole profile. Error bars are standard deviations.

Earth Surface Processes and Landforms, 2012, http://dx.doi.org/10.1002/esp.3220

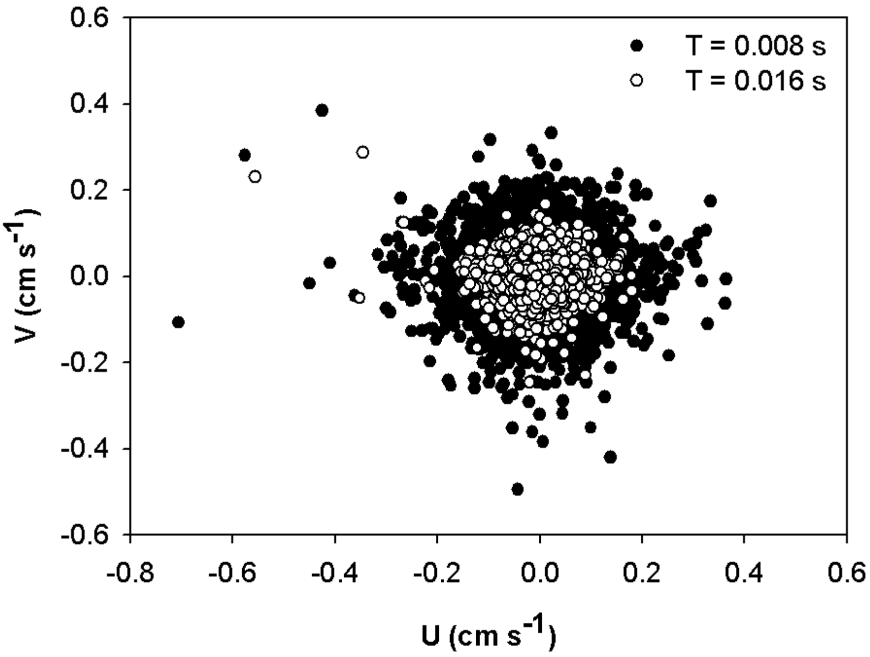

Figure 6: Values of velocity components *U* and *V*, along *X*- and *Y*-axes respectively, obtained with the LSPIV procedure on dry zones during flowing experiments on the sinusoidal surface. The image processing was performed with a time interval between two images (*T*) of 0.008 or 0.016 s.

Earth Surface Processes and Landforms, 2012, http://dx.doi.org/10.1002/esp.3220

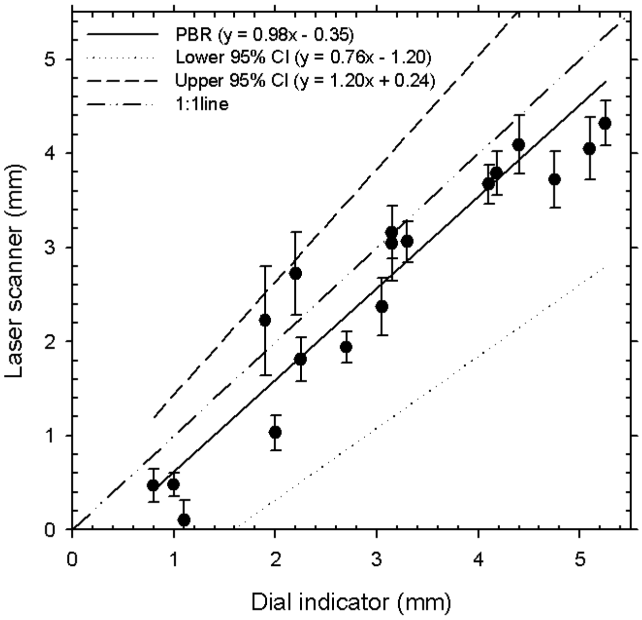

Figure 7: Comparison of water depth measurements with dial indicator and with laser scanner on the sinusoidal surface. Error bars are standard deviations. Equations in parentheses correspond to the Passing Bablok regression (PBR) line and the associated confidence intervals (CI).

Earth Surface Processes and Landforms, 2012, http://dx.doi.org/10.1002/esp.3220

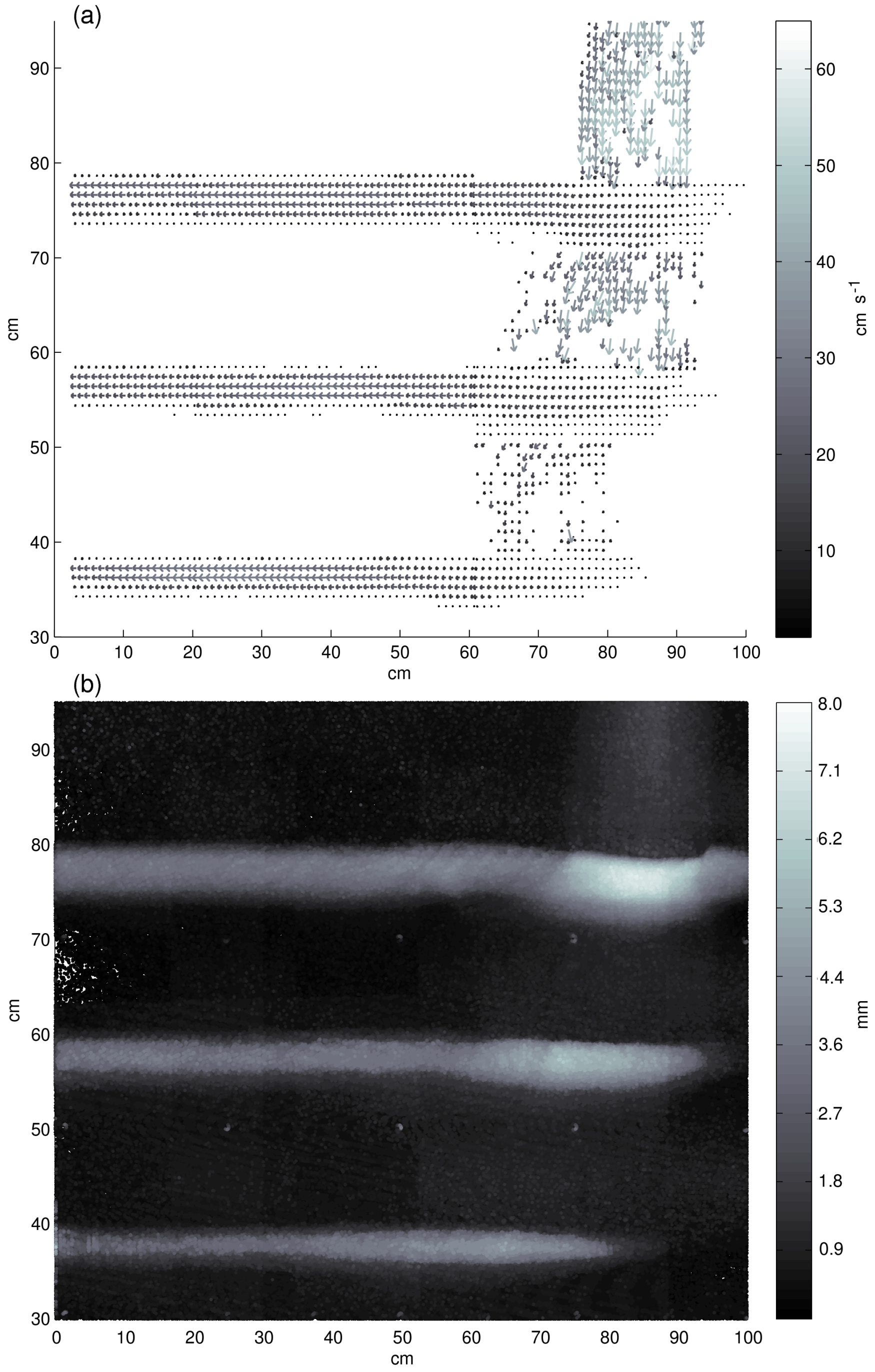

Figure 8: Measurements of (a) flow velocity and (b) water depth for experiment D with three corrugations outflowing from the sinusoidal surface.

Earth Surface Processes and Landforms, 2012, http://dx.doi.org/10.1002/esp.3220

Figure 9: Velocity (LSPIV) and water depths (laser scanner) measured on various transects of each corrugation of the sinusoidal surface for two experiments. (a) Three outlets were active only on one side of the surface (Up, Central and Down). (b) All six outlets were flowing (i.e. both ends of each corrugation).

Earth Surface Processes and Landforms, 2012, http://dx.doi.org/10.1002/esp.3220

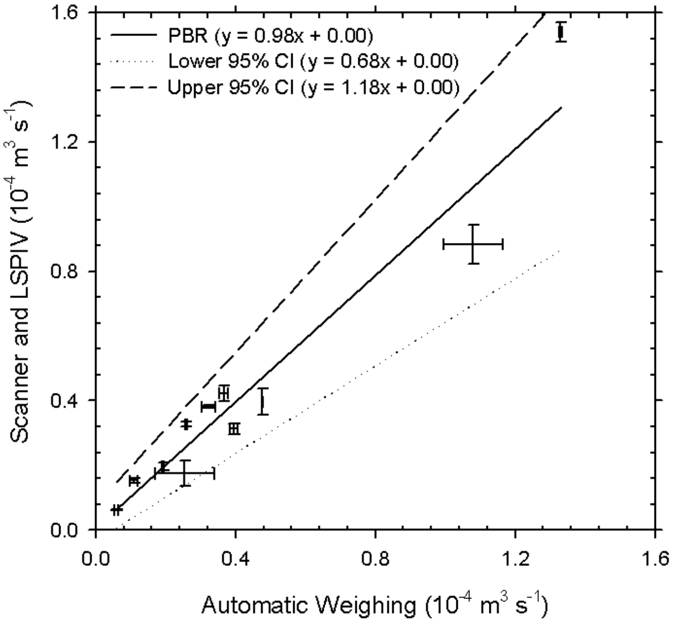

Figure 10: Comparison of flow rates obtained from automatic weighing and from the combination of laser scanner and LSPIV measurements for each corrugation on the sinusoidal surface. Error bars are standard deviations. Equations in parentheses correspond to the Passing Bablok regression (PBR) line and the associated confidence intervals (CI).